

# Similar modes of polypeptide recognition by export chaperones in flagellar biosynthesis and type III secretion

Artem G Evdokimov<sup>1,2</sup>, Jason Phan<sup>1</sup>, Joseph E Tropea<sup>1</sup>, Karen M Routzahn<sup>1</sup>, Howard K Peters III<sup>1</sup>, Matthew Pokross<sup>1,2</sup> & David S Waugh<sup>1</sup>

**Assembly of the bacterial flagellum and type III secretion in pathogenic bacteria require cytosolic export chaperones that interact with mobile components to facilitate their secretion. Although their amino acid sequences are not conserved, the structures of several type III secretion chaperones revealed striking similarities between their folds and modes of substrate recognition. Here, we report the first crystallographic structure of a flagellar export chaperone, *Aquifex aeolicus* FliS. FliS adopts a novel fold that is clearly distinct from those of the type III secretion chaperones, indicating that they do not share a common evolutionary origin. However, the structure of FliS in complex with a fragment of FliC (flagellin) reveals that, like the type III secretion chaperones, flagellar export chaperones bind their target proteins in extended conformation and suggests that this mode of recognition may be widely used in bacteria.**

Assembly of the bacterial flagellum is a complex process that must proceed in a precise temporal order<sup>1</sup>. First, the basal components FlgE, FlgK and FlgL are assembled inside the bacterial membrane. Next, the filament cap protein FliD is exported. Finally, about 20,000 FliC (flagellin) monomers are sequentially secreted through the channel and polymerized to form the tail filament. The export and assembly process is regulated in part by the association of these structural proteins with cognate export chaperones in the bacterial cytosol. Export chaperones FlgN, FliT and FliS bind specifically to FlkK or FlgL, FliD and FliC, respectively<sup>2,3</sup>. It is thought that a principal function of the export chaperones is to prevent premature interactions between structural components of the bacterial flagellum in the cytosol<sup>4,5</sup>.

FlgN, FliT and FliS do not share any obvious amino acid sequence similarity, but all three are acidic polypeptides of approximately the same size (~120–140 residues) that reportedly function as homodimers<sup>3,6</sup>. In these respects, the flagellar chaperones resemble the export chaperones for cytotoxic effector proteins that are injected into eukaryotic cells by type III secretion systems of pathogenic bacteria<sup>4</sup>. Yet, there are also differences between these two types of export chaperones. Whereas type III secretion chaperones bind to sites near the N termini of their cognate effectors, flagellar export chaperones interact with the C termini of their binding partners. Moreover, unlike the type III secretion chaperones, there is no compelling evidence that the flagellar export chaperones play a direct role in the secretion process *per se*. Nevertheless, considering that many structural components of the type III secretion apparatus have homologs in the bacterial flagellum<sup>7,8</sup>, we thought it plausible that the flagellar export chaperones and the type III secretion chaperones may have similar structures. This

could not be ascertained simply by comparing their amino acid sequences, because the sequences of the type III secretion chaperones SycE, SicP, SigE and CesT are not conserved yet all four proteins adopt very similar folds<sup>9–13</sup>. Therefore, to determine whether flagellar export chaperones are structural relatives of the type III secretion chaperones, we crystallized and determined the structure of the flagellar export chaperone FliS.

## RESULTS

### The structure of FliS

The flagellum has been studied most extensively in enteric bacteria. However, efforts to obtain crystals of *Escherichia coli* and *Vibrio cholerae* FliS proteins were unsuccessful. This prompted us to try a more phylogenetically divergent ortholog from the hyperthermophilic bacterium *Aquifex aeolicus*. *A. aeolicus* FliS readily yielded crystals that diffracted X-rays to a resolution of 2.2 Å. The structure was solved by the single isomorphous replacement and anomalous scattering (SIRAS) technique, using a mercury derivative.

The structure of FliS is an embellished, antiparallel four-helix bundle with a quasi-helical cap on one end formed by the 16 N-terminal residues (Fig. 1a). The closest structural relatives are other helical bundles (such as cytochromes), but none of these bear more than a vague resemblance to FliS. A search of the coordinates available from the Protein Data Bank with the program Dali<sup>14</sup> identified *Salmonella typhimurium* CheA, a five-helix bundle, as the most similar structure (*Z*-score = 9.0). The structure of FliS (Fig. 1b) is obviously unrelated to those of the type III secretion chaperones, as exemplified by *Yersinia pestis* SycE<sup>10</sup> (Fig. 1c). Thus, although there are a number of

<sup>1</sup>Macromolecular Crystallography Laboratory, Center for Cancer Research, National Cancer Institute at Frederick, PO Box B, Frederick, Maryland 21702-1201, USA.

<sup>2</sup>Present address: Procter & Gamble Pharmaceuticals, Health Care Research Center-Discovery, 8700 Mason-Montgomery Road, Mason, Ohio 45040-9462, USA. Correspondence should be addressed to D.W. (waughd@ncicrf.gov).

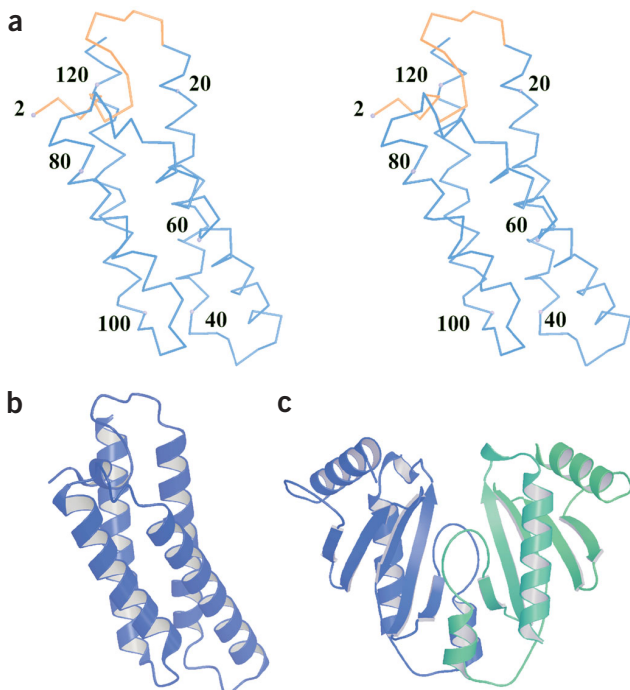


**Figure 1** The structure of *Aquifex aeolicus* FliS is unrelated to those of the type III secretion chaperones. (a) Stereo view of the C $\alpha$  trace of FliS. The N-terminal residues that are absent from the electron density maps in two of the four protomers that comprise the asymmetric unit of the crystal are orange. (b) Ribbon model of FliS. (c) Ribbon model of *Yersinia pestis* SycE<sup>10</sup>, with each subunit of the homodimer in a different color.

superficial similarities between flagellar export chaperones and the type III secretion chaperones, they clearly do not share a common evolutionary origin.

Like the type III secretion chaperones, *Salmonella enterica* FliS was reported to be a homodimer in solution<sup>3</sup>. Yet, judging by its behavior on a gel filtration column and from dynamic light scattering (DLS) measurements, *A. aeolicus* FliS seems to be a monomeric protein. Moreover, none of the interactions between FliS molecules in the crystal lattice is extensive enough to suggest that they may be biologically relevant. Although it is conceivable that two distantly related orthologs could have different quaternary structures, we do not believe that this is the case because the FliS proteins from *V. cholerae* and *E. coli*, two very close relatives of *S. enterica*, behaved very much like *A. aeolicus* FliS on a high resolution Superdex-75 gel filtration column and DLS measurements indicated that these proteins are also monomers in solution (data not shown). Furthermore, the counterparts of all 40 amino acids that comprise the FliS binding site of *S. enterica* FliC<sup>15</sup> are bound by a single FliS polypeptide in the crystal structure of the *A. aeolicus* FliS–FliC complex (see below).

### FliS forms a stable complex with FliC

*S. enterica* FliS binds to the C terminus of FliC<sup>3,15</sup>. To confirm that the His<sub>6</sub>-tagged form of *A. aeolicus* FliS is a functional protein, we co-expressed it in *E. coli* with the 91 C-terminal residues of *A. aeolicus* FliC (FliC(427–518)). The two polypeptides associated with one another to form a stable complex that persisted during purification on immobilized metal affinity chromatography (IMAC), ion exchange, hydroxyapatite and gel filtration columns (Fig. 2).

We were unable to crystallize this FliS–His<sub>6</sub>–FliC(427–518) complex. Reasoning that the fragment of FliC we selected might be longer than necessary and therefore partially disordered, we subjected the complex to limited proteolysis (Fig. 2), an approach that enabled the type III secretion chaperones SicP and SycE to be cocrystallized with fragments of their cognate effectors<sup>12,16</sup>. The FliS–FliC complex was more resistant to the action of thermolysin than was FliS alone. One of the principal thermolysin digestion products of the FliS–FliC complex was identified by mass spectrometry and N-terminal amino acid sequencing as residues 465–518 of FliC. Accordingly, we next attempted to co-express *A. aeolicus* FliC(464–518) with FliS–His<sub>6</sub>. To eliminate a truncated form of FliS–His<sub>6</sub> that copurified with FliC(427–518) and was impossible to remove under non-denaturing conditions (Fig. 2), Met12 of FliS was replaced with a glutamine residue (M12Q). Glutamine occurs frequently at this position in FliS proteins from other organisms.

The FliS(M12Q)–His<sub>6</sub>–FliC(464–518) complex was overproduced in *E. coli* and purified to homogeneity by IMAC and gel filtration. The final preparation did not contain any truncated FliS. Like FliC(427–518), FliC(464–518) also bound tightly to FliS(M12Q)–His<sub>6</sub>, indicating that this fragment of FliC does indeed include the FliS binding site and demonstrating that the M12Q mutation does not interfere with the formation of the complex (data not shown).

### Structure of FliS in complex with a fragment of FliC

We succeeded in growing crystals of the FliS(M12Q)–His<sub>6</sub>–FliC(464–518) complex that diffracted to a resolution of 2.5 Å, and we solved the structure by molecular replacement, using the structure of FliS–His<sub>6</sub> as a search model. The hydrodynamic radius of the FliS(M12Q)–His<sub>6</sub>–FliC(464–518) complex, estimated by DLS measurements, is consistent with a stoichiometry of 1:1, and this is also what we observed in the crystal structure. Residues 479–518 of FliC are wrapped around the outside of FliS in an extended, horseshoe-like conformation with secondary (helical) but no tertiary structure (Fig. 3a). This general mode of polypeptide binding is similar to the way in which the type III secretion chaperones interact with their cognate effectors, as exemplified by the structure of the *Yersinia pseudotuberculosis* SycE–YopE complex<sup>16</sup> (Fig. 3b).

About 40 residues of FliC and 50 residues of YopE interact with FliS and SycE in their respective complexes, burying a comparable molecular surface area of 3,670 Å<sup>2</sup> (FliS–FliC) and 4,570 Å<sup>2</sup> (SycE–YopE). The interface between FliS and FliC is dominated by hydrophobic interactions

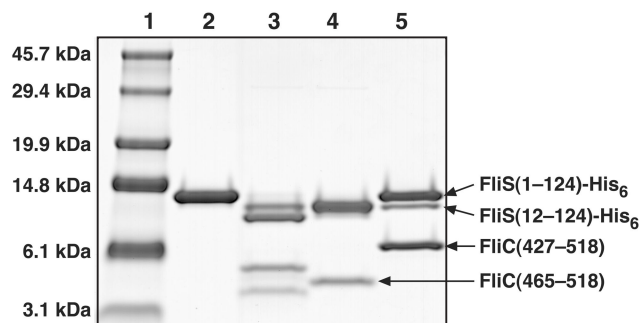


**Figure 2** Limited proteolysis of FliS–His<sub>6</sub> in the presence and absence of FliC(427–518). Lane 1, molecular mass standards. Lane 2, FliS(1–124)–His<sub>6</sub>. Lane 3, FliS(1–124)–His<sub>6</sub> treated with thermolysin. Lane 4, FliS(1–124)–His<sub>6</sub>–FliC(427–518) complex treated with thermolysin. Lane 5, FliS(1–124)–His<sub>6</sub>–FliC(427–518) complex. The concentration of thermolysin used in this experiment was 6.25 μg ml<sup>-1</sup>.

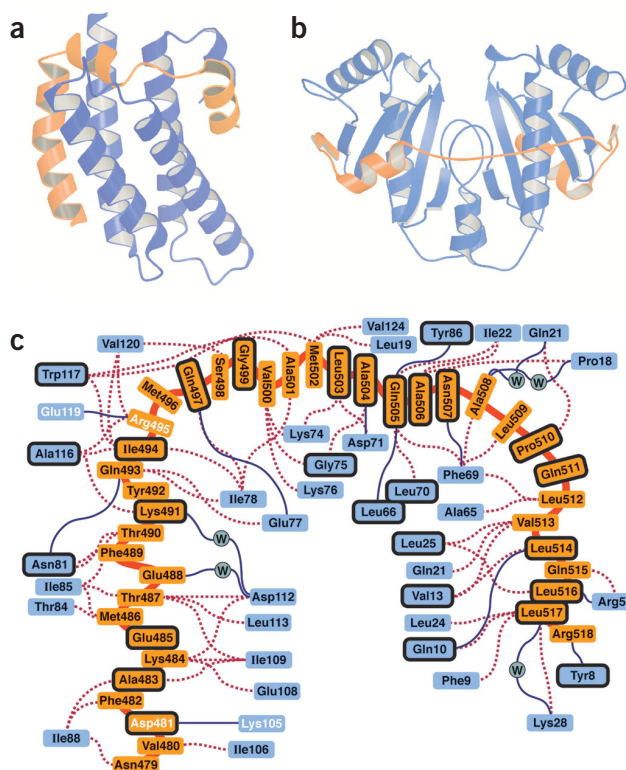


(Fig. 3c), as is also the case in the SycE–YopE complex. There are only nine side chain–mediated hydrogen bonds and two (FliS–FliC) or three (SycE–YopE) intermolecular salt bridges in each complex. Apart from these generalities, the precise way in which the FliC and YopE polypeptides are bound by their respective chaperones is not the same. This is not surprising in view of the fact that there is no sequence or structural similarity between FliS and SycE or their cognate binding partners.

There are no significant differences between the conformations of SycE in its complexed and uncomplexed states. By contrast, a substantial conformational change in FliS accompanies the binding of FliC. Two of the four protomers in the asymmetric unit of the FliS crystal have disordered N termini, whereas in the other two molecules the 15 N-terminal residues form a quasi-helical cap on one end of the helical bundle (Fig. 1a). This suggests that the N-terminal cap is loosely bound and can dissociate from the remainder of the protein without causing it to unfold. Indeed, upon binding to FliC the N-terminal cap of FliS is displaced and reorganized to form a short helix on one side of the bundle (Fig. 3a). In this new conformation, a groove is created to bind one of the  $\alpha$ -helical segments of FliC (residues 510–518). At the same time, the adjacent helical segment of FliC (residues 499–505) moves into the position formerly occupied by the helical cap on FliS, where Gln505 of FliC closely mimics the hydrogen bonding interactions formed by Tyr8 in the capped conformation of FliS. In fact, Ala7–Tyr8 of FliS and Ala504–Gln505 of FliC occupy equivalent positions (Fig. 4). Thus, the N terminus of FliS appears to act as a ‘molecular stopper’ to plug the hydrophobic binding site when FliS is not bound to FliC.

## DISCUSSION

### FliS and FliC interact via conserved surfaces

Alignments of FliS and FliC sequences from phylogenetically diverse bacteria (Fig. 5) indicate that most of the amino acids in *A. aeolicus*

**Figure 3** FliS and SycE bind their targets in an extended conformation. (a) The structure of FliS (blue) in complex with residues 464–518 of FliC (orange). (b) The structure of SycE (blue) in complex with residues 17–85 of YopE (orange)<sup>16</sup>. (c) Schematic representation of the interactions between FliS and FliC. The orange line and boxes represent the polypeptide backbone and individual amino acid residues of FliC, respectively. Blue boxes, FliS residues. The residues that form intermolecular salt bridges have white labels. Broken red lines, intermolecular van der Waals interactions; solid blue lines, intermolecular hydrogen bonds. Green circles, water molecules. Highly conserved residues in FliS and FliC (defined in Fig. 5) have bold outlines.

FliS that interact with FliC are conserved, especially Tyr8 and the residues that form the binding pocket for Gln505 in FliC (or Tyr8 in FliS), suggesting that the ‘stopper’ mechanism can be generalized to FliS proteins from other bacteria. Similarly, those amino acids in *A. aeolicus* FliC that contact FliS also tend to be well conserved, including Gln505 and the adjacent residues, which make the greatest number of intermolecular atomic contacts with FliS (Fig. 5b). It therefore seems likely that the interaction between FliS and FliC proteins from other bacteria will closely resemble the structure of the *Aquifex* FliS–FliC complex described here.

The overall degree of sequence conservation between the C termini of FliC proteins is greater than that exhibited by their FliS counterparts, most likely because this region of FliC carries out a dual function; it not only interacts with FliS but also mediates polymerization of the flagellar tail filament. This may explain why some of the residues in FliC that do not contact FliS are also highly conserved. The particularly high degree of conservation among FliS residues that form the binding pocket for Gln505 of FliC, together with the high density of intermolecular contacts in this region of the complex (Fig. 5b), suggests that Gln505 is a key binding determinant. However, this residue is not conserved in FliC proteins from all organisms (such as *E. coli* and *Shigella flexneri*). Except for the conservative replacement of Ile22 by valine, all of the residues that form the binding pocket for Gln505 in *A. aeolicus* FliS are the same in the *E. coli* and *S. flexneri* proteins.

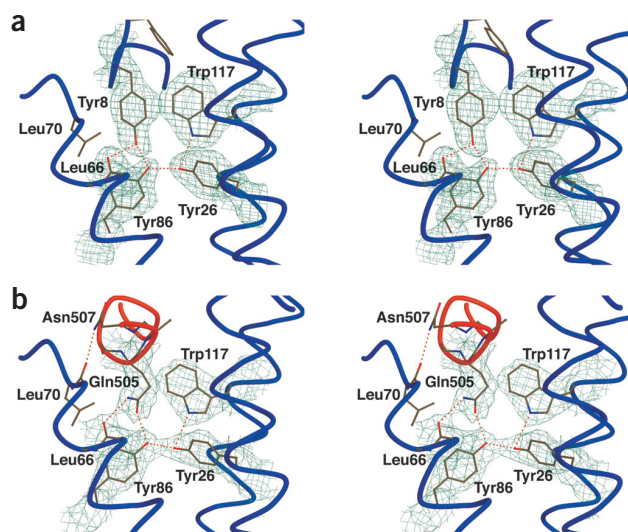


**Figure 4** Gln505 of FliC and Tyr8 of FliS occupy equivalent positions in the hydrophobic pocket of FliS. (a) Intramolecular interactions involving Tyr8 in the structure of FliS. (b) Intermolecular interactions between Gln505 of FliC and FliS. Hydrogen bonds are indicated by dashed lines.  $2F_o - F_c$  composite-omit electron density is contoured at  $1.2\sigma$ .

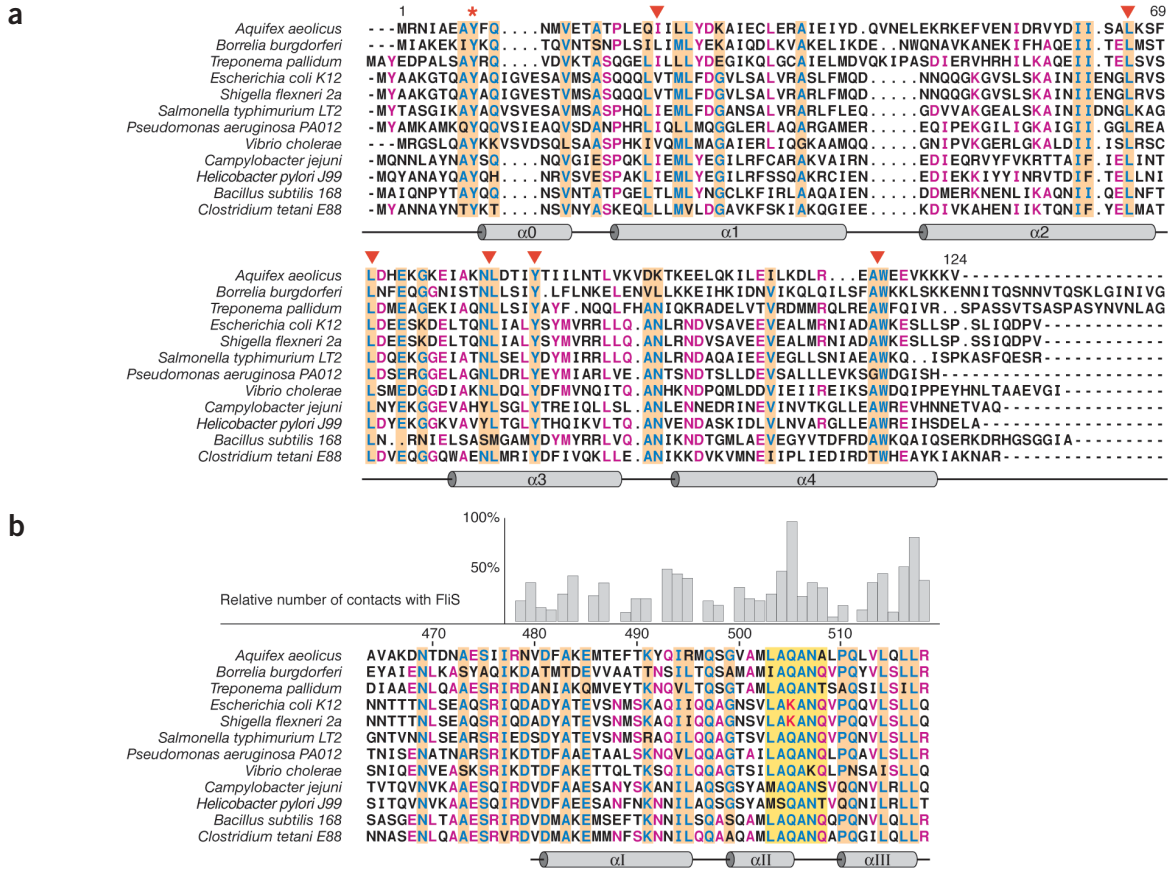


**Figure 5** Structure-based sequence alignments of FliS and FliC proteins from various bacterial species with residues numbered according to the *A. aeolicus* proteins. (a) FliS. (b) FliC. Only the C-terminal 55 residues of the FliC sequences are shown. Moderately conserved residues (identical in at least 6 of the 12 sequences) are magenta, and highly conserved residues (identical in at least 9 of the 12 sequences) are blue on brown background. Tyr8 of FliS is marked with a red asterisk and FliS residues that contact Gln505 of FliC in the FliS–FliC complex are marked with red triangles. Secondary structure elements are shown schematically under the alignments. The FliC sequences are aligned with a histogram that indicates the relative number (%) of intermolecular contacts made by each residue in FliC, normalized such that 100% of Gln505 is considered to contact FliS. The residues in FliC that interact with the hydrophobic pocket of FliS are shown on a yellow background. The lysine residues in *E. coli* and *S. flexneri* FliC that occupy the same position as Gln505 in *A. aeolicus* FliC are red.

Consequently, it is unclear what compensatory changes in FliS, if any, are required to accommodate a positively charged lysine side chain in the pocket normally occupied by polar glutamine or tyrosine (in FliS) residues.

### Biological implications

FliS and the type III secretion chaperones use different structural solutions to achieve a similar task: binding polypeptides in an extended, nonglobular conformation. Yet, it is unlikely that these two types of protein–protein complexes play analogous roles in type III secretion and flagellar biosynthesis. There is ample evidence that the type III secretion chaperones facilitate the secretion of their cognate binding partners, either by maintaining them in a partially unfolded state that is primed for export<sup>12</sup>, or by actively delivering them to the secretion apparatus<sup>16</sup>. By contrast, FliS does not seem to be directly involved in the secretion of FliC. Rather, its function is to prevent the premature polymerization of FliC in the bacterial cytosol. Indeed, the C terminus of FliC, which corresponds to the FliS binding site, is the key to the polymerization of this molecule<sup>17</sup>. The crystal structure of the FliS–FliC complex does not suggest how the C terminus of FliC polymerizes. Although it is conceivable

that polymerization is mediated somehow by the three  $\alpha$ -helices observed in the cocrystal structure with FliS, it is also possible that the conformation of polymerized FliC is entirely different.

In conclusion, we have demonstrated that although their modes of polypeptide binding are strikingly similar, FliS-related flagellar export chaperones do not share a common evolutionary origin with the type III secretion chaperones. Rather, it seems that they arose independently, after the divergence of the ancestral export machinery that gave rise to the flagellum and the type III secretion systems. It remains to be seen if, like their counterparts in type III secretion systems, the three flagellar export chaperones FliS, FliT and FlgN also have similar tertiary structures. Although the amino acid sequences of FliT and FlgN are consistent with an  $\alpha$ -helical fold, they seem to be unrelated to that of FliS. The conservation of structurally important residues in sequences from a multitude of bacteria suggests that the general architecture of the *A. aeolicus* FliS and FliS–FliC structures is also broadly conserved.

### METHODS

**Protein expression and purification.** The open reading frame encoding *A. aeolicus* FliS was amplified from genomic DNA by PCR and inserted by recombi-

**Table 1** Essential crystallographic parameters

	FliS	FliS + Hg (4 sites)	FliS–FliC
Space group	$P2_12_12$	$P2_12_12$	$I4_132$
Cell dimensions (Å)			
<i>a</i>	87.07	85.61	166.24
<i>b</i>	131.76	132.44	166.24
<i>c</i>	74.90	74.86	166.24
Resolution (Å) <sup>a</sup>	100–2.2 (2.3–2.2)	100–2.7 (2.8–2.7)	100–2.5 (2.7–2.5)
Completeness <sup>a</sup>	94.9 (94.3)	93.2 (92.8)	99.4 (99.9)
Redundancy <sup>a</sup>	3.25 (2.29)	2.81 (2.19)	4.4 (4.8)
Unique reflections <sup>a</sup>	44,213 (5,127)	22,390 (2,184)	13,539 (1,492)
<i>I</i> / $\sigma I$ <sup>a</sup>	13.64 (3.65)	19.63 (5.82)	16.54 (2.79)
$R_{\text{merge}}$ (%) <sup>a,b</sup>	4.73 (28.5)	4.60 (17.0)	4.45 (36.7)
$R_{\text{ano}}$ (%)	–	8.5	–
$R_{\text{native/derivative}}$ (%)	–	16.4	–
Figure of merit <sup>c</sup>	0.35 (0.71)	–	–
$R_{\text{all}}$ (%) <sup>d</sup>	23.3	–	22.4
$R_{\text{free}}$ (%) <sup>d</sup>	28.6	–	24.7
R.m.s. deviation			
Bond length (Å)	0.05	–	0.06
Bond angle (°)	1.7	–	2.1
Ramachandran			
Preferred (%)	96.1	–	94.1
Allowed (%)	3.9	–	5.9

<sup>a</sup>Values in parentheses are for the highest resolution shell. <sup>b</sup> $R_{\text{merge}} = \sum |I_i - \langle I \rangle| / \sum I_i$  where  $I_i$  is the intensity of the  $i^{\text{th}}$  observation and  $\langle I \rangle$  is the mean intensity of the reflections. <sup>c</sup>Value in parentheses is after density modification with two-fold NCS averaging. <sup>d</sup> $R = \sum |F_o| - |F_c| / \sum |F_o|$ , crystallographic *R*-factor, and  $R_{\text{free}} = \sum |F_o| - |F_c| / \sum |F_o|$  where all reflections belong to a test set of randomly selected data.

torial cloning into the pDEST-14 expression vector (Invitrogen) to create pKM1234. A His<sub>6</sub>-tag was added to the C terminus of FliS during PCR amplification. FliS-His<sub>6</sub> was produced in *E. coli* BL21 (DE3) cells that also contained the tRNA accessory plasmid pRIL (Stratagene), grown overnight at 37 °C without induction. The crude cell extract was incubated at 70 °C to precipitate endogenous proteins, and then the FliS-His<sub>6</sub> was purified by IMAC, ion exchange (Mono-Q) and gel filtration (Superdex-75) chromatography. The vector used to co-express FliC(427–518) with FliS-His<sub>6</sub> (pKM1310) was constructed by Gateway multisite recombinatorial cloning (Invitrogen). The first open reading frame in the bicistronic mRNA encoded residues 427–518 of *A. aeolicus* FliC fused to the C terminus of *E. coli* maltose binding protein (MBP) and the second reading frame encoded FliS-His<sub>6</sub>. The MBP fusion protein was cleaved *in vivo* by TEV protease<sup>18</sup> before purification of the FliS-His<sub>6</sub>–FliC(427–518) complex. The same approach was used to co-express residues 464–518 of FliC with FliS(M12Q)-His<sub>6</sub> (pKM1384), except that in this case FliC was not produced as an MBP fusion protein. The FliS-His<sub>6</sub>–FliC(427–518) complex was purified by IMAC, hydroxyapatite, ion exchange (Q-Sepharose) and gel filtration (Superdex-75) chromatography. The FliS(M12Q)-His<sub>6</sub>–FliC(464–518) complex was purified by IMAC and gel filtration.

**Limited proteolysis and identification of fragments.** The FliS-His<sub>6</sub>–FliC(427–518) complex (3 mg ml<sup>-1</sup>) was incubated at 37 °C for 60 min in the presence of varying concentrations of thermolysin (Boehringer-Mannheim) in 10 mM Tris-HCl (pH 8.0), 2 mM CaCl<sub>2</sub>, 1.4 mM 2-mercaptoethanol, 200 mM NaCl, 5% (v/v) glycerol. The reaction products were analyzed by electrospray mass spectrometry, using an Agilent 1100 Series LC/MSD. In some cases, protein bands were electrophoretically transferred from SDS gels to PVDF membranes and subjected to N-terminal amino acid sequencing.

**Crystallization, data collection and structure determination.** FliS-His<sub>6</sub> was crystallized by the hanging-drop vapor diffusion technique. The best crystals were obtained with 10 mg ml<sup>-1</sup> FliS-His<sub>6</sub> in 20 mM MES (pH 6.5), 150 mM NaCl, 2 mM DTT (buffer A) set as 3 μl:3 μl (protein/reservoir) drops against a reservoir solution containing 2.0 M ammonium sulfate, 100 mM MES or cacodylate buffer (pH 5.4–6.2). Cryoprotection was difficult, but successful flash freezing (nitrogen stream at 100 K) could be carried out after a 10 s immersion of the crystals in a mixture of 2.0 M ammonium sulfate, pH 6.0 (MES), 100 mM nondetergent sulfobetaine-201, 15% (w/v) sucrose and 20% (v/v) ethylene glycol. The structure was

solved by SIRAS using a mercury derivative obtained by cocrystallization of the protein with 0.1 mM ethyl mercury phosphate. The FliS-His<sub>6</sub>–FliC(464–518) complex was crystallized using 15–30 mg ml<sup>-1</sup> protein solution in buffer A, set as 3 μl:3 μl drops against 10–12% (v/v) isopropanol, 250 mM Li<sub>2</sub>SO<sub>4</sub>, 100 mM citrate-phosphate buffer (pH 4.0–4.5). Crystals were flash frozen after brief immersion into 27% (v/v) methyl pentanediol, 12% (v/v) isopropanol, 400 mM Li<sub>2</sub>SO<sub>4</sub>, pH 4.2 (citrate-phosphate buffer). The structure was solved by molecular replacement (AMoRe<sup>19</sup>), using the FliS-His<sub>6</sub> monomer as a search model. Molecular models of the FliS-His<sub>6</sub> and FliS-His<sub>6</sub>–FliC(464–518) structures were built manually with the program O<sup>20</sup> and refined with SHELX-97 (ref. 21) and REFMAC<sup>22</sup>. The essential data collection and refinement statistics are given in Table 1.

**Coordinates.** The coordinates and structure factors for *A. aeolicus* FliS-His<sub>6</sub> and FliS-His<sub>6</sub>–FliC(464–518) have been deposited in the Protein Data Bank (accession codes 1ORJ and 1ORY, respectively).

#### ACKNOWLEDGMENTS

We thank SBL Biophysics Core Resource (US National Cancer Institute at Frederick) for the use of the electrospray mass spectrometer and the Protein Chemistry Laboratory (SAIC-Frederick) for amino acid sequencing. Data were collected at beamlines 17-ID and 17-BM in the facilities of the Industrial Macromolecular Crystallography Association Collaborative Access Team (IMCA-CAT) at the Advanced Photon Source.

#### COMPETING INTERESTS STATEMENT

The authors declare that they have no competing financial interests.

Received 7 March; accepted 25 July 2003

Published online at <http://www.nature.com/naturestructuralbiology/>

- Aldridge, P. & Hughes, K.T. Regulation of flagellar assembly. *Curr. Opin. Microbiol.* **5**, 160–165 (2002).
- Fraser, G.M., Bennett, J.C.Q. & Hughes, C. Substrate-specific binding of hook-associated proteins by FlgN and FliT, putative chaperones for flagellum assembly. *Mol. Microbiol.* **32**, 569–580 (1999).
- Auvray, F., Thomas, J., Fraser, G.M. & Hughes, C. Flagellin polymerisation control by a cytosolic export chaperone. *J. Mol. Biol.* **308**, 221–229 (2001).
- Bennett, J.C.Q. & Hughes, C. From flagellum assembly to virulence: the extended family of type III export chaperones. *Trends Microbiol.* **8**, 202–204 (2000).
- Page, A.-L. & Parsot, C. Chaperones of the type III secretion pathway: jacks of all trades. *Mol. Microbiol.* **46**, 1–11 (2002).
- Bennett, J.C.Q., Thomas, J., Fraser, G.M. & Hughes, C. Substrate complexes and domain organization of the *Salmonella* flagellar export chaperones FlgN and FliT. *Mol. Microbiol.* **39**, 781–791 (2001).
- Macnab, R.M. The bacterial flagellum: reversible rotary propeller and type III export apparatus. *J. Bacteriol.* **181**, 7149–7153 (1999).
- Nguyen, L., Paulsen, I.T., Tchiew, J., Hueck, C.J. & Saier, M.H. Jr. Phylogenetic analyses of the constituents of type III protein secretion systems. *J. Mol. Microbiol. Biotechnol.* **2**, 125–144 (2000).
- Birtalan, S. & Ghosh, P. Structure of the *Yersinia* type III secretory system chaperone SycE. *Nat. Struct. Biol.* **8**, 974–978 (2001).
- Evdokimov, A.G., Tropea, J.E., Routzahn, K.M., & Waugh, D.S. Three-dimensional structure of the type III secretion chaperone SycE from *Yersinia pestis*. *Acta Crystallogr. D* **58**, 398–406 (2002).
- Trame, C.B. & McKay, D.B. Structure of the *Yersinia enterocolitica* molecular-chaperone protein SycE. *Acta Crystallogr. D* **59**, 389–392 (2003).
- Stebbins, C.E. & Galan, J.E. Maintenance of an unfolded polypeptide by a cognate chaperone in bacterial type III secretion. *Nature* **414**, 77–81 (2001).
- Luo, Y. *et al.* Structural and biochemical characterization of the type III secretion chaperones CesT and SigE. *Nat. Struct. Biol.* **8**, 1031–1036 (2001).
- Holm, L. & Sander, C. Protein structure comparison by alignment of distance matrices. *J. Mol. Biol.* **233**, 123–138 (1993).
- Ozin, A.J., Claret, L., Auvray, F. & Hughes, C. The FliS chaperone selectively binds the disordered flagellin C-terminal D0 domain central to polymerisation. *FEMS Microbiol. Lett.* **219**, 219–224 (2003).
- Birtalan, S., Phillips, R.M. & Ghosh, P. Three-dimensional secretion signals in chaperone-effector complexes of bacterial pathogens. *Mol. Cell* **9**, 971–980 (2002).
- Samatey, F.A. *et al.* Structure of the bacterial flagellar protofilament and implications for a switch for supercoiling. *Nature* **410**, 331–337 (2001).
- Kapust, R.B. & Waugh, D.S. Controlled intracellular processing of fusion proteins by TEV protease. *Prot. Expr. Purif.* **19**, 312–318 (2000).
- Navaza, J. AmoRe: an automated package for molecular replacement. *Acta Crystallogr. D* **50**, 157–163 (1994).
- Jones, T.A., Zou, J.Y., Cowan, S.W. & Kjeldgaard, M. Improved methods for building protein models in electron density maps and the location of errors in these models. *Acta Crystallogr. A* **47**, 110–119 (1991).
- Sheldrick, G.M. & Schneider, T.R. SHELXL: high-resolution refinement. *Methods Enzymol.* **277**, 319–343 (1997).
- Vagin, A.A. & Dodson, E.J. Refinement of macromolecular structures by the maximum-likelihood method. *Acta Crystallogr. D* **53**, 240–255 (1997).